Optimal path planning in a constant wind with a bounded turning rate

Timothy G. McGee,* Stephen Spry † and J. Karl Hedrick‡
Center for Collaborative Control of Unmanned Vehicles, University of California, Berkeley, CA 94720

In this paper, we explore the problem of generating the optimal time path from an initial position and orientation to a final position and orientation in the two-dimensional plane for an aircraft with a bounded turning radius in the presence of a constant wind. Following the work of Boissonnat, we show using the Minimum Principle that the optimal path consists of periods of maximum turn rate or straight lines. We demonstrate, however, that unlike the no wind case, the optimal path can consist of three arcs where the length of the second arc is less than π. A method for generating the optimal path is also presented which iteratively solves the no wind case to intercept a moving virtual target.

I. Introduction

Optimal path planning is an important problem for robotics and unmanned vehicles. In this paper, we explore a method for finding the shortest path from an initial position and orientation to a final position and and orientation in the two-dimensional plane for an aircraft with a bounded turning radius in the presence of a constant wind. This work was motivated by our group's work with our fleet of small autonomous aircraft. Each modified Sig Rascal aircraft flies under the combined control of an off-the-shelf Piccolo avionics package for low level control and an onboard PC104 computer for higher level tasks. These aircraft fly at a nominal speed of 20 m/s, and wind speeds of over 5 m/s have been encountered during flight testing.

The problem described above was first solved in the case of no wind by Dubins using geometric arguments[8] and later by Boissonnat using optimal control methods.[4,6] The solution of this problem for the no wind case has also been used for higher level path planning of mobile robots[9,10] and to travel around obstacles.[1,3] Similar work has been done investigating the rendezvous of a robotic manipulator with moving objects[7] and on path planning and trajectory generation for coordinated rendezvous of multiple unmanned aerial vehicles (UAVs).[2]

A. Vehicle Kinematic Model

The kinematic model considered is shown below. The control input of the aircraft, u, is the turning rate, $\dot{\psi}$, which is assumed to be bounded $|\dot{\psi}| < \dot{\psi}_{max}$. V_a is the constant velocity of the aircraft, and V_W is the constant velocity of the wind, with $V_a > V_W$.

$$\mathbf{x} = \begin{bmatrix} x \\ y \\ \psi \end{bmatrix} \qquad \dot{\mathbf{x}} = \begin{bmatrix} V_a \cos\psi + V_{Wx} \\ V_a \sin\psi + V_{Wy} \\ u \end{bmatrix} \tag{1}$$

These equations of motion can be expressed in a more compact way without loss of generality by defining $\psi = 0$ in the direction of the wind and normalizing:

*Graduate Student, Department of Mechanical Engineering, tmcgee@me.berkeley.edu
†Postdoctoral Researcher, Department of Mechanical Engineering, sspry@me.berkeley.edu
‡Professor, Department of Mechanical Engineering, khedrick@me.berkeley.edu

$$\dot{\mathbf{x}} = \begin{bmatrix} cos\psi + \beta \\ sin\psi \\ u \end{bmatrix} \tag{2}$$

where $|u| < \dot{\psi}_{max}$ and $|\beta| < 1$ is the ratio of the wind speed to the aircraft speed.

B. Orientation Angle vs. Velocity Direction

The goal of the optimization problem is to find the shortest path from $\mathbf{x}_i = (x_i, y_i, \psi_i)$ to $\mathbf{x}_f = (x_f, y_f, \psi_f)$ in the plane. It should be noted that in the presence of wind, the direction of the velocity vector is not equal to the heading angle, ψ. The direction of the velocity vector, α, can be defined as:

$$\alpha = atan2\left(\frac{\dot{y}}{\dot{x}}\right) = atan2\left(\frac{sin\psi}{cos\psi + \beta}\right) \tag{3}$$

where the $atan2$ function preserves the quadrant of the angle by accounting for the sign of the numerator and denominator. Thus, if one wishes to find the optimal path from an initial position and velocity direction (x_i, y_i, α_i) to a final position and velocity direction (x_f, y_f, α_f), each α can be converted to the corresponding ψ by

$$\psi = acos(-\beta sin\alpha) - \frac{\pi}{2} + \alpha \tag{4}$$

where the value of the acos function is chosen so that $\psi > 0$ if $\alpha > 0$.

C. Expressing the Problem as one with a Moving Virtual Target

The original problem of finding an optimal path in the presence of a constant wind can be re-expressed as one of finding the optimal path from an initial position and orientation with no wind to a final orientation over a moving virtual target. The velocity of the virtual target is equal and opposite to the velocity of the wind. The path of the aircraft in this redefined problem is its path with respect to the moving air frame, and will be referred to as the "air path". If this path is flown in the presence of wind, the path of the aircraft with respect to the ground will be known as the "ground path". The new equations of motion for the redefined problem become:

$$\mathbf{x} = \begin{bmatrix} x \\ y \\ \psi \end{bmatrix} \qquad \dot{\mathbf{x}} = \mathbf{f}(x, u) = \begin{bmatrix} \cos\psi \\ \sin\psi \\ u \end{bmatrix} \tag{5}$$

and with $\mathbf{x}_i$ given. We seek to find the input such that $\mathbf{x}(T) = \mathbf{x}_d(T)$, where

$$\mathbf{x}_d(t) = \begin{bmatrix} x_f - \beta t \\ y_f \\ \psi_f \end{bmatrix} \tag{6}$$

.

II. Minimum Principle

Following the work of Boissonnat,[4] insight into the problem can be gained through the application of classical optimal control theory. Using the notation of Bryson and Ho,[5] we first define the performance index, J, which is equal to the intercept time, T:

$$J = \int_0^T L\, dt = \int_0^T 1\ dt = T \tag{7}$$

In order to enforce the maximum turning radius of the vehicle, the dynamics of Eq. 5 are adjoined to the performance index with a multiplier $\boldsymbol{\lambda}$ to form the Hamiltonian, H:

$$H = L + \boldsymbol{\lambda}^T \mathbf{f} = 1 + \lambda_1 \cos\psi + \lambda_2 \sin\psi + \lambda_3 u \tag{8}$$

where the dynamics of the multiplier satisfies:

$$\dot{\boldsymbol{\lambda}} = -\frac{dH}{d\mathbf{x}} = -\begin{bmatrix} 0 & 0 & 0 \\ 0 & 0 & 0 \\ -\sin\psi & \cos\psi & 0 \end{bmatrix} \tag{9}$$

By defining the Hamiltonian and multiplier dynamics in this way, the Minimum Principle requires that on the optimal trajectory, $(\mathbf{x}^*, \boldsymbol{\lambda}^*)$, the optimal control, u^* must minimize H over the set of all possible inputs, u_a, at each instance in time:

$$H(\mathbf{x}^*, u^*, \boldsymbol{\lambda}^*, t) \leq H(x^*, u, \lambda^*, t) \quad \forall \quad u \in u_a, t \in [0, T] \tag{10}$$

Since λ_1 and λ_2 are constant as shown in Eq. 9, satisfying the condition in Eq. 10 is equivalent to satisfying:

$$\lambda_3 u^* \leq \lambda_3 u \quad \forall \quad |u| \leq \dot{\psi}_{max} \tag{11}$$

These necessary conditions lead to several properties that the optimal solution must have.

Property 1 *The optimal path consists of intervals of maximum rate turns and straight lines.*

Proof: First, we note again that λ_1 and λ_2 are constants and that λ_3 is a continuous function whose time derivative is zero whenever $\sin\psi\lambda_1 = \cos\psi\lambda_2$. Given λ_1 and λ_2, this equation can be used to define a characteristic direction ψ_c. During any non-zero time interval, λ_3 is constant if and only if travel is in a straight line parallel to the characteristic direction. Now, the optimality condition in Eq. 11 allows only three input values, dictated by the value of λ_3: on any segment having $\lambda_3 > 0$, $u^* = -\dot{\psi}_{max}$; on any segment having $\lambda_3 < 0$, $u^* = \dot{\psi}_{max}$; on any segment having $\lambda_3 \equiv 0$, we must have travel in a straight line, implying $u^* = 0$.

Property 2 *All straight segments and changes in turning direction on the optimal path must occur on a single line in the plane.*

Proof: As shown by Boissonnat,[4] using $\dot{x} = \cos\psi$ and $\dot{y} = \sin\psi$, the equation for $\dot{\lambda}_3$ becomes $\dot{\lambda}_3 = \dot{y}\lambda_1 - \dot{x}\lambda_2$, which integrates to

$$c = \lambda_3 + x\lambda_2 + y\lambda_1 \tag{12}$$

where c is a constant. For fixed values of c, λ_1, and λ_2, each value of λ_3 defines one of a family of lines, all parallel to the characteristic direction, ψ_c, in the x, y plane. The line defined by $\lambda_3 = 0$ is the line on which all switching and straight-line travel must occur.

Property 3 *The characteristic line defined in Property 2 divides the plane into two regions such that when following the optimal path, the aircraft executes a maximum right turn in one of the regions and a maximum left turn in the other region.*

Proof: Without loss of generality, we write λ_1 and λ_2 as $\lambda_1 = q\cos\psi_c$ and $\lambda_2 = q\sin\psi_c$ for some constant q. We define the characteristic unit vector $\mathbf{e}_c$ and the perpendicular unit vector $\mathbf{e}_p$ as:

$$\mathbf{e}_c = \begin{bmatrix} \cos\psi_c \\ \sin\psi_c \end{bmatrix} \qquad \mathbf{e}_p = \begin{bmatrix} -\sin\psi_c \\ \cos\psi_c \end{bmatrix} \tag{13}$$

We also define the vehicle velocity vector $\mathbf{v}$ and the wind velocity vector $\mathbf{v}_w$ as:

$$\mathbf{v} = \begin{bmatrix} \cos\psi \\ \sin\psi \end{bmatrix} \qquad \mathbf{v}_w = \begin{bmatrix} \beta \\ 0 \end{bmatrix} \tag{14}$$

In terms of these vectors, we have

$$\begin{bmatrix} \lambda_1 \\ \lambda_2 \end{bmatrix} = q\mathbf{e}_c \tag{15}$$

and

$$\dot{\lambda}_3 = q\mathbf{v}^T\mathbf{e}_p \tag{16}$$

Integrating Eq. 16, with the knowledge that $\lambda_3 = 0$ on the characteristic line, shows that $\lambda_3 = qd_c$, where d_c is the signed distance from the current aircraft position to the characteristic line. This shows that λ_3 is always positive on one side of the characteristic line and negative on the other. Combined with the optimality conditions, this implies that the input value is always minimum on one side of the line and maximum on the other, corresponding to maximum left and right turns.

Property 4 *All intersections of the optimal path with the characteristic line will occur at the same angle.*

Proof: On any optimal path, the time derivative of the Hamiltonian is given by

$$\dot{H} = H_t + H_u\dot{u} = \lambda_3\dot{u} \tag{17}$$

Since $\dot{u} = 0$ on all segments, H is piecewise constant. Since $\lambda_3 u$ is continuous, H is also continuous and thus a constant. Combining Eqs. 8, 14, and 15, H can be written in the form

$$H = 1 + q\mathbf{v}^T\mathbf{e}_c + \lambda_3 u \tag{18}$$

Since H is constant, this implies that whenever $\lambda_3 = 0$, $\mathbf{v}^T\mathbf{e}_c$ and thus the angle that the aircraft intercepts the characteristic line are also constant. This also implies that any path that meets the characteristic line at a non-zero angle can have no straight segments.

III. Strategy for Generating Minimum Paths

While the application of the Minimum Principle gives insight into the nature of the solution, it does not provide a method for actually solving for the paths. For the no wind case of the problem, the generation of candidate paths using maximum turns and straight lines is straightforward since it involves only calculating tangents to circles. If a constant wind is added, however, the ground path of the aircraft becomes a much more complicated shape, and the generation of paths consisting of maximum rate turns and straight lines is more difficult. This problem can be addressed by iteratively solving for the optimal paths using the problem formulation with a virtual moving target outlined above. Under the virtual target formulation, the final position of the aircraft is that of a virtual target moving in a straight line. Any point along this line can be expressed by a single variable d which is the distance to the initial target position. We can define two functions $T_a(d)$ and $T_{vt}(d)$ where T_a is the time it takes the aircraft to fly the optimal air path from its initial position and orientation to a final orientation at point d, and T_{vt} is the time it takes the virtual target to move to point d. The goal of the optimization problem is then to find the smallest d at which $T_a(d) = T_{vt}(d)$. This approach is very similar to that used by Croft to calculate rendezvous of a manipulator with moving objects.[7] The $T_a(d)$ function can be generated by calculating the length of each of the admissible Dubins path types (RSR,LSL, RSL, LSR, RLR_{outer}, LRL_{outer}) and letting T_a equal the minimum of these lengths divided by the constant vehicle speed. For these six path types, R denotes a right turn with a minimum radius of curvature, L a left turn with minimum radius of curvature, and S a straight line. The outer subscript indicates that the arc length of the center curve is greater than π. The RLR_{outer} and LRL_{outer} curves only exist when the centers of the outer circles are less than $4R_{min}$ apart, and the LSR and RSL only exist when the outer circles have centers greater than $2R_{min}$ apart. Examples of the six types of admissible paths are shown in Figure 1 for $\mathbf{x}_i = (0, 0, 0)$ and $\mathbf{x}_f = (2.5, .5, -\pi)$.

We next define a new function $G(d)$ which is the difference of $T_a(d)$ and $T_{vt}(d)$. By calculating where $G(d) = 0$, we find points where the aircraft will intercept the virtual moving target.

$$G(d) \stackrel{\text{def}}{=} T_a(d) - T_{vt}(d) \tag{19}$$

Remark 1 *G(d) is piecewise continuous, and all discontinuities occur when the RSL and LSR paths fail to exist.*

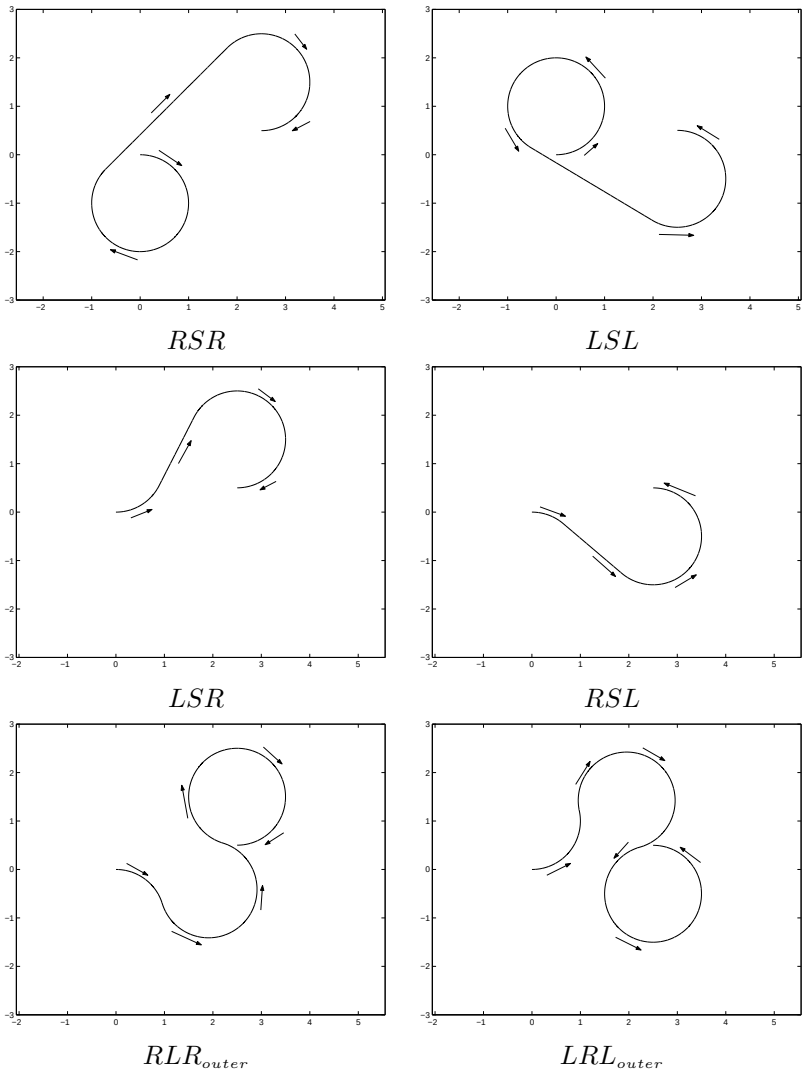

Figure 1. Example of six admissible Dubins paths.

Proof: It was shown by Bui[6] that the length of the optimal path is piecewise continuous in the no-wind case, and that discontinuities occur when the RSL and LSR paths fail to exist. Since the virtual target follows a continuous path, the difference of $T_a(d)$ and $T_{vt}(d)$ must also be piecewise continuous.

An example of the discontinuity is shown in Figure 2. For this example, $\mathbf{x}_i = (0, 0, 0)$ and $\mathbf{x}_f = \{(1.95, 2, 0), (2.05, 2, 0)\}$. Note that a small shift in the final position to the right produces a discontinuity in the optimal path length when the LSR curve comes into existence.

Remark 2 $G(0) > 0$ *and* $lim_{d\to\infty}(G(d)) < 0$.

Proof: $T_{vt}(0) = 0$ since the virtual target is already at point d, and $T_a(0) > 0$ since the aircraft requires some positive time to fly to any point different from its own starting point. Thus $T_a(0) - T_{vt}(0) > 0$. As d approaches ∞, the majority of the path of the aircraft is a straight line that is nearly parallel to the path of the virtual target. Since $|\beta| < 1$, if d is made large enough, the aircraft will always reach point d before the virtual target, making $G(d) < 0$.

Given Remark 2, it is clear that $G(d)$ must either equal zero or have a discontinuity across zero for at least one value of d. For given initial and final positions and orientations, the resulting $G(d)$ function can thus be

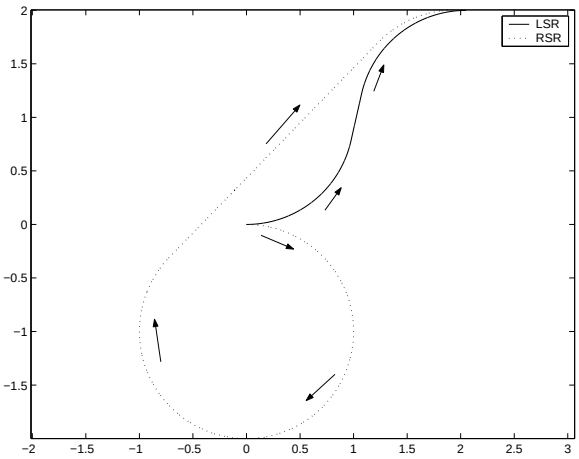

Figure 2. Discontinuity in optimal path length for small change in final position.

classified as one of two types.

Type 1 *This first type of function consists of all $G(d)$ functions such that $G(d) = 0$ at some $d = d^*$, and $G(d) > 0$ for all $d < d^*$.*

Examples of plots of Type 1 are shown in Figure 3.

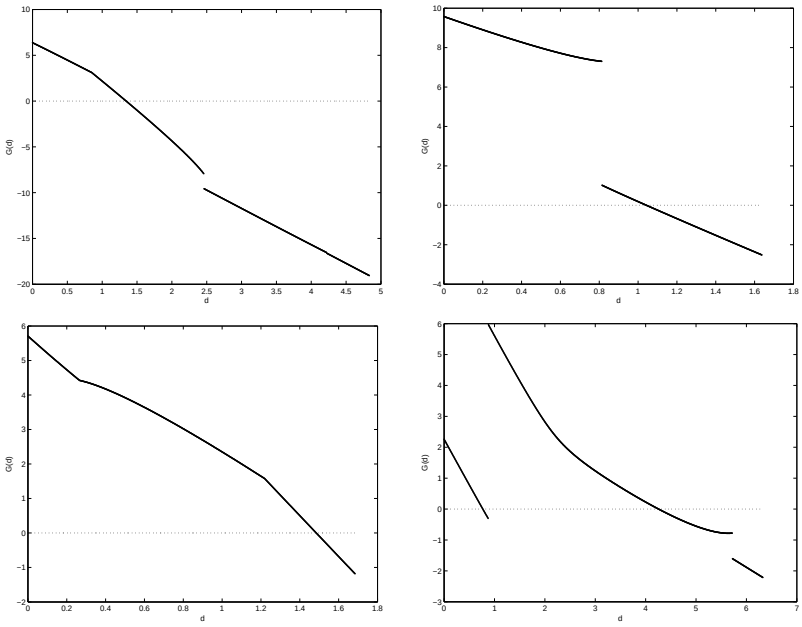

Figure 3. Examples of $G(d)$ functions of Type 1.

Type 2 *This second category consists of any functions that do not belong to the first.*

Examples of plots of Type 2 are shown in Figure 4.

Remark 3 *For any $G(d)$ function of Type 1, the point d^* represents the first point at which the aircraft can intercept the virtual target at the specified final orientation.*

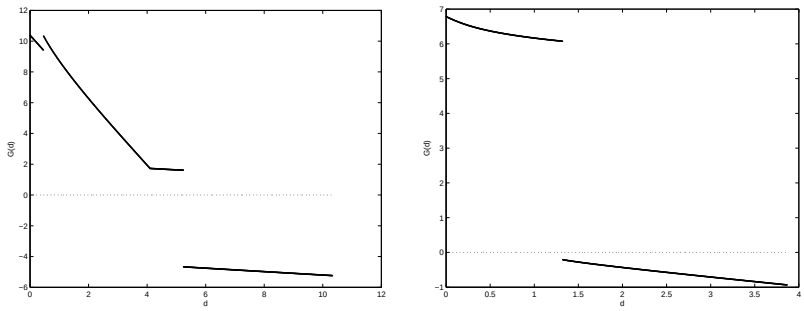

Figure 4. Examples of $G(d)$ functions of Type 2.

Proof: Assume d^* is not the first point at which the aircraft can intercept the virtual target. Thus there is some $\hat{d} < d^*$ such that $G(\hat{d}) = 0$. However, by the definition of Type 1, $G(d) > 0$ for all $d < d^*$. Thus by contradiction d^* is the first point at which the aircraft can intercept the virtual target.

Remark 4 *The existence of the Type 2 functions for $G(d)$ implies that for some initial and final positions and orientations, the aircraft must fly a non minimum distance air path to the optimal interception point on the path of the virtual target.*

Proof: The $G(d)$ function is calculated using the optimal aircraft path to each point d. Thus if the $G(d)$ function is never equal to zero, the aircraft can never intercept the virtual target by flying an optimal air path.

Remark 4 implies that for some boundary conditions, the aircraft must fly a longer air path to the optimal interception point in order to allow the virtual target to catch up. From the use of the Minimum Principle, we know that in order to optimally intercept the target, the aircraft can only use straight lines and arcs of minimum turning radius. The first option to do this is to use one of the longer Dubins paths. For example in Figure 1, the LSR path is the shortest, and the remaining paths shown are the longer Dubins paths. The second option is to introduce RLR_{inner} and LRL_{inner} curves where the inner subscript refers to the fact that the second curve has an angle less than π. Examples of these lengthened air paths are shown below in Figure 5. In order to further analyze the problem with the addition of these extra path types, we now define a new family of functions:

$$G_X(d) \stackrel{\text{def}}{=} T_{Xa}(d) - T_{vt}(d) \tag{20}$$

where X denotes the type of path including the six Dubins paths (RSR, RSL, etc.) and the additional RLR_{inner} and LRL_{inner} paths, and $T_{Xa}(d)$ denotes the time it takes the aircraft to fly to a specific point d on the virtual target path using that specific path type. It is important to note that not all eight of the $G_X(d)$ functions are defined for every value of d. Examples of these $G_X(d)$ functions are shown below in Figure 6.

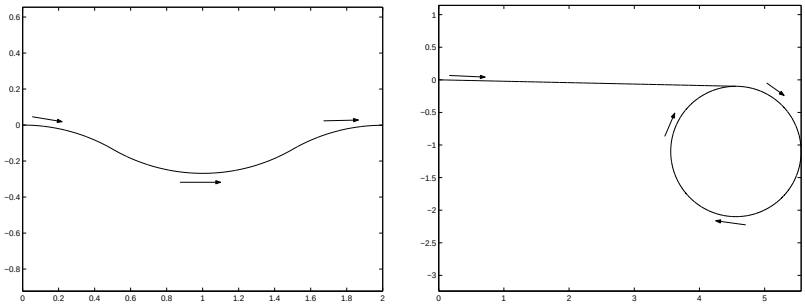

Figure 5. Examples of lengthened air paths to a given d.

Remark 5 *If there is a $G(d)$ function of Type 2, there will be either a RLR_{outer}, LRL_{outer}, RLR_{inner} or LRL_{inner} path that intercepts the virtual target.*

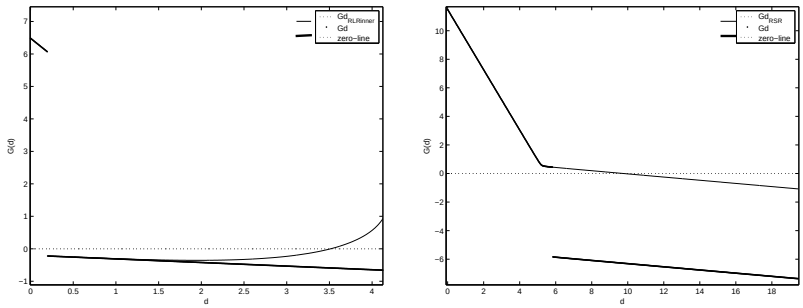

Figure 6. Examples of $G_{RLR_{inner}}(d)$ and $G_{RSR}(d)$ functions.

Proof: Consider the case where the jump across zero occurs when the LSR path comes into existence. Before the jump, $G_{LRL_{outer}}(d) > 0$ since $G(d) > 0$ and $G_{LRL_{outer}}(d) \geq G(d)$. At the jump discontinuity $G_{LRL_{inner}}(d) < 0$ because the LRL_{inner} path is equivalent to the LSR path. This occurs because the length of the second left arc in the LRL_{inner} path is equal to zero, and the straight portion of the LSR path is equal to zero. This leaves two LR paths which are equivalent. As d increases, the centers of the two left arcs in the LRL_{outer} and LRL_{inner} curves move further apart. When the two centers are exactly $4R_{min}$ apart, the LRL_{outer} and LRL_{inner} curves are equivalent, and the arc length center curve is π. Because $G_{LRL_{outer}}(d) > 0$ and $G_{LRL_{inner}}(d) < 0$ and they converge to the same value, one of them must cross zero. This convergence is illustrated in Figure 7.

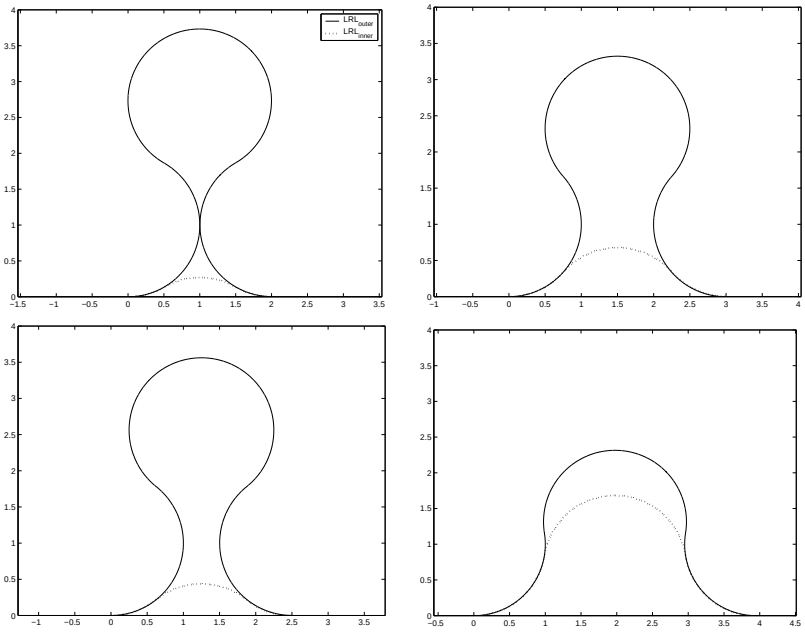

Figure 7. Convergence of LRL_{inner} and LRL_{outer} paths.

Remark 6 *The optimal path from $\mathbf{x}_i$ to $\mathbf{x}_f$ for a aircraft with a minimum turning radius in the presence of a constant wind will be one of the following set of curves {RSR, LSL, RSL, LSR, LRL_{outer}, RLR_{outer}, LRL_{inner},, RLR_{inner}, $SR_{2\pi}S$, or $SL_{2\pi}S$).*

Proof: It was shown using optimal control methods that the optimal path consists of periods of maximum turning rate and straight lines. It was also shown that for boundary conditions which produce Type 1 $G(d)$ functions, the optimal path is one of the standard Dubins curves. For Type 2 paths, the discontinuity occurs when either a RSL or LSR comes into existence, producing a jump of less than $2\pi R_{min}$. The optimal

rendezvous point with the virtual target will be found by either using the shortest path that doesn't cause a discontinuity, which is one of the longer Dubins paths, or by lengthening the RSL or LSR path that produced the discontinuity. The most that a RSL or LSR path can be lengthened without increasing the length of the curve more than $2\pi R_{min}$ is to use a LRL_{inner} or RLR_{inner} path. Finally, Remark 5 guarantees that one of these types of curves will always intercept the virtual target.

The $SL_{2\pi}S$ and $SR_{2\pi}S$ paths can be thought of as limiting cases for RSR and LSL where one of the curves approaches zero arc length and the second curve approaches an arc length of 2π. These path types are optimal for only a small set of boundary conditions where the initial and final heading angles must be identical. An example of this is when $\mathbf{x}_i = (0, 0, 0)$ and $\mathbf{x}_f = (-5.5, 0, 0)$ with β = -.9. This corresponds to a aircraft with a final position directly behind the initial position flying into a strong headwind. The optimal path in this case is to fly a full circle and a very short straight section into the wind (in the direction of the virtual target path). The straight section of this path can be divided arbitrarily before and after the full circle. Examples of these paths are shown in Figure 8. Notice that the boundary conditions and path lengths are equivalent. While paths of type $SR_{2\pi}S$ or $SL_{2\pi}S$ are discussed here for completeness, they can be disregarded in practice by always changing ψ_i or ψ_f by a negligible random amount if they are ever equal. This will cause any possible $SR_{2\pi}S$ or $SL_{2\pi}S$ path to become a RSR or LSL path.

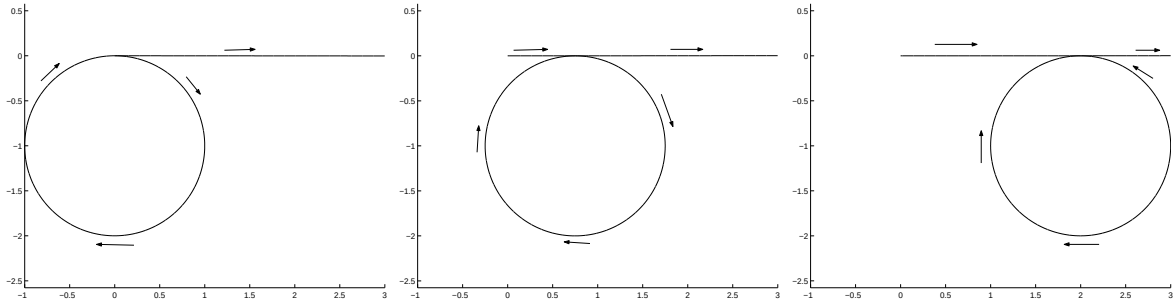

Figure 8. Example of $SR_{2\pi}S$ paths.

IV. Final Solution Strategy

Solving for $G(d) = 0$ is not adequate to find the optimal path for all sets of boundary conditions since it fails for functions of Type 2. In order to overcome this, a $G_X(d)$ function can be created for each path type in the extended set of Remark 6. For each of these functions, the d^* values are calculated where that function is equal to zero. The optimal path is chosen as the curve which produces the smallest d^*. The d^* values can calculated using a variety of standard iterative root finding methods such as a bisection algorithm or gradient descent algorithm.

V. Examples

Several examples of optimal paths in the presence of wind are shown in Figures 9, 10, 11, and 12. For Figure 9, $\mathbf{x}_i = (0, 0, \pi/2)$ and $\mathbf{x}_f = (-1.5, -2, 0)$. For Figure 10, $\mathbf{x}_i = (0, 0, \pi/4)$ and $\mathbf{x}_f = (5, 1, \pi)$. In these first two examples, the optimal rendezvous paths are LRL_{outer} and RSR respectively, and represent cases that produce Type 1 $G(d)$ functions. The second two examples illustrate boundary conditions that produce Type 2 $G(d)$ functions. For Figure 11, $\mathbf{x}_i = (0, 0, 0)$, $\mathbf{x}_f = (-5.5, 2, 0)$, and the rendezvous path is a RSR path which is a lengthened air path. For Figure 12, $\mathbf{x}_i = (0, 0, 0)$, $\mathbf{x}_f = (-.43, .56, 0)$, and the rendezvous path is of type LRL_{inner}.

VI. Conclusions and Future Work

A study of the problem of finding the optimal path from an initial position and orientation to a final position and orientation for an aircraft with a limited turning radius in the presence of a constant wind has been presented. It was shown that the set of admissible optimal paths is greater than in the case with no

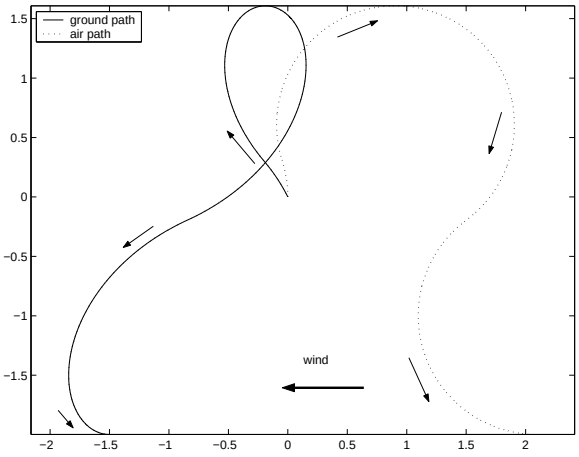

Figure 9. Example of optimal LRL_{outer} path in presence of wind $\beta = -0.5$.

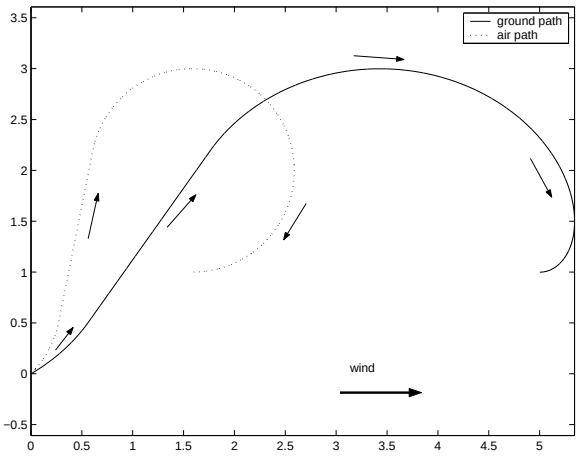

Figure 10. Example of optimal LSR path in presence of wind $\beta = 0.5$.

wind. An iterative method for solving for the paths has also been presented and several examples of optimal paths in the presence of wind have been presented. Current work is being done to implement this algorithm on our actual fleet of aircraft to optimally visit a set of points in a constant wind. In order to account for small variability in the wind, a turning rate less than the actual maximum turning rate will be used to calculate a near optimal path. This near optimal path can then be used as a trajectory that can be followed in the presence of disturbances.

Acknowledgments

This work was supported by the ONR grant #N00014-03-C-0187, SPO #016671-004 and a Berkeley Fellowship for Mr. McGee.

References

[1]Pankaj K. Agarwal, Prabhakar Raghavan, and Hisao Tamakai. Motion planning for a steering-constrained robot through moderate obstacles. In *Proceedings of the Twenty-Seventh Annual ACM Symposium on the Theory of Computing*, 1995.

[2]Randal W. Beard, Timothy W. McLain, and Michael Goodrich. Coordinated target assignment and intercept for unmanned air vehicles. In *Proceedings of the 2002 IEEE International Conference on Robotics and Automation*, 2002.

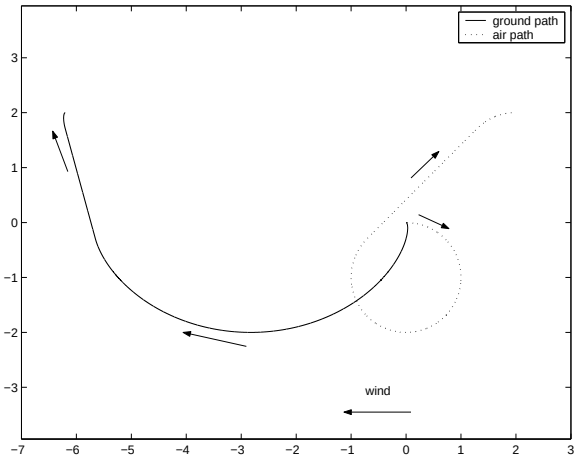

Figure 11. Example of optimal RSR path in presence of wind $\beta = -0.9$.

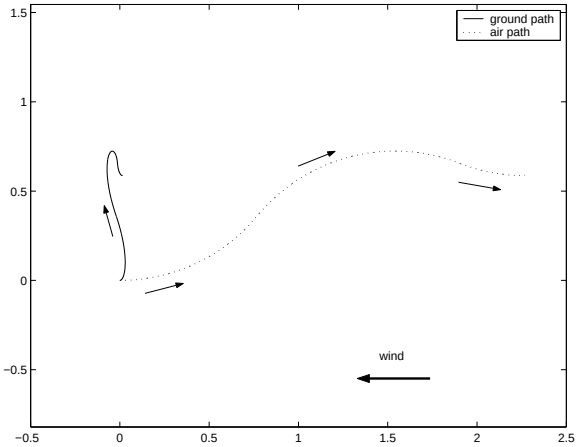

Figure 12. Example of optimal LRL_{inner} path in presence of wind $\beta = -0.9$.

[3]Antonio Bicchi, Giuseppe Casalino, and Corrado Santilli. Planning shortest bounded-curvature paths for a class of nonholonomic vehicles among obstacles. *Journal of Intelligent and Robotic Systems*, 16, 1996.

[4]Jean-Daniel Boissonnat, Andre Cerezo, and Juliette Leblond. Shortest paths of bounded curvature in the plane. In *Proceedings of the 1992 IEEE Int. Conf. on Robotics and Automation*, 1992.

[5]Arthur Bryson and Yu-Chi Ho. *Applied Optimal Control: Optimization, Estimation, and Control*. John Wiley and Sons, New York, New York, 1975.

[6]Xuan-Nam Bui, Jean-Daniel Boissonnat, Philippe Soueres, and Jean-Paul Laumond. Shortest path synthesis for dubins non-holonomic robot. In *Proceedings of the 1994 IEEE Int. Conf. on Robotics and Automation*, 1994.

[7]Elizabeth Croft, R.G. Fenton, and Beno Benhabib. Optimal rendezvous-point selection for robotic interception of moving objects. *IEEE Transactions on Systems, Man, and Cybernetics–PartB: Cybernetics*, 28, 1998.

[8]L.E. Dubins. On curves of minimal length with a constraint on average curvature, and with prescribed initial and ternminal positions and tangents. *American Journal of Mathmatics*, 79, 1957.

[9]Zhijun Tang and Umit Ozguner. On motion planning for multi-target surveillance with limited resources of mobile sensor agents. Accepted to the IEEE Journal of Robotics, 2004.

[10]Guang Yang and Vikram Kapila. Optimal path planning for unmanned air vehicles with kinematic and tactical constraints. In *Proceedings of the 41st IEEE Int. Conf. on Decision and Control*, 2002.